

Resolution of the binding configuration in nitrogen-doped carbon nanotubes

L. H. Chan, K. H. Hong, D. Q. Xiao, T. C. Lin, S. H. Lai, W. J. Hsieh, and H. C. Shih*

Department of Materials Science and Engineering, National Tsing Hua University, Hsinchu, Taiwan 300, Republic of China

(Received 22 April 2003; revised manuscript received 8 March 2004; published 13 September 2004)

Nitrogen-doped carbon nanotubes (N-doped CNTs) were synthesized by exposing CNTs under high input power nitrogen plasma (3.1 kW), using a microwave plasma enhanced chemical vapor deposition system. In the analysis of high resolution transmission electron microscopy, it was found that graphene layers of the N-doped CNTs became seriously curved, waved, or buckled, and even contained fullerene-like structures, in contrast to the parallel concentric graphene layers in the normal CNTs. X-ray photoelectron spectroscopy (XPS) and electron energy loss spectroscopy (EELS) were combined to resolve the binding configurations of nitrogen and carbon in the N-doped CNTs. In the XPS study, it may be concluded that the N-doped CNTs have three binding configuration types (poly 4-vinylpyridine, poly 9-vinylcarbazole, and poly aniline oligomer) using the method proposed by [F. L. Normand, J. Hommet, T. Szörényi, C. Fuchs, and E. Fogarassy, *Phys. Rev. B* **64**, 235416 (2001)] EELS results showed that the incorporation of nitrogen into the CNTs would induce sp^2 binding for carbon atoms, similar to the results in amorphous carbon nitride films [J. Hu, P. Yang, and C. M. Leiber, *Phys. Rev. B* **57**, 3185 (1998); C. Ronning, H. Feldermann, R. Merk, and H. Hofsäs, *Phys. Rev. B* **58**, 2207 (1998)]. N $1s$ core-level downshift of ~ 1 eV in the XPS analyses was mainly caused by the screening effects of core holes in the π bond around nitrogen atoms.

DOI: 10.1103/PhysRevB.70.125408

PACS number(s): 81.07.De, 61.48.+c, 78.30.Na, 61.46.+w

I. INTRODUCTION

Since carbon nanotubes (CNTs) were first discovered in 1991,⁴ extensive research on carbon nanotubes and other related nanoscale materials have been carried out throughout the scientific world. There are many processes to synthesize CNTs, including electric arc discharge, laser ablation, catalytic chemical vapor deposition, and plasma assisted chemical vapor deposition, as well as others.⁵ It has been well known that the electronic structures of CNTs are closely dependent on the size and chirality, which are not easily controlled in the synthesis process. An extrinsic atomic doping method provides a splendid way to tune and optimize the electronic properties of CNTs. For example, boron-doped CNTs are metallic intrinsically predicted by the theoretical calculations⁶ and experimentally proved by conductivity measurements,⁷ nevertheless the conductivity of CNTs could be metallic or semiconducting depending on their chirality. In the academic research on doped CNTs, boron and nitrogen atoms are the two most widely used atomic species applied to investigate the evolution of the nanostructures, chemical binding configurations, physical, and electronic properties resulting from the doping.⁸⁻¹¹ Due to a small difference in atomic radii, it is quite easy for B or N atoms to substitute C atoms in the hexagonal graphene structures of CNTs. In addition, different from other carbon-based materials such as graphite, diamond, and carbon films, the surface to volume ratio of CNTs is so high that large specific surface areas can serve as the reaction sites to assist the foreign atoms in substituting the carbon atoms.^{12,13} Similar to the semiconducting materials, B- or N-doped carbon can be used to manufacture *p*-type or *n*-type CNTs (or nanowires), and to fabricate nanoscaled electronic devices by proper junction of these two types.

Although there are abundant results for B-doped or N-doped CNTs to date, the analysis for chemical binding

configurations of nitrogen in N-doped CNTs is still lacking detailed and converged conclusions, especially in the x-ray photoelectron spectroscopy (XPS) investigation. To study the binding configurations of the N-doped CNTs, we invoked the published XPS analysis results and theoretical calculation of the amorphous carbon nitride films and N-doped carbon related nanomaterials as references, and made some reasonable modifications by combining the electron energy loss spectroscopy (EELS) measurements, Fourier transform infrared spectroscopy (FTIR), and the characteristic nanostructures of CNTs.

Liu and Cohen^{14,15} theoretically predicted the existence of the covalent β - C_3N_4 with the mechanical properties similar to the diamond, which triggered many experimental efforts on the synthesis of the carbon nitride films.¹⁶⁻¹⁸ XPS, EELS, and FTIR are generally used as the analytical tools in order to investigate the binding structures of carbon nitride films. Due to the lack of suitable standard samples for reference, XPS results of carbon nitride films were published with diverse conclusions from group to group, even leading to contradictory arguments. Marton and co-workers¹⁹ used three and four lines to fit the N $1s$ and C $1s$ core-level spectra, respectively. They applied two phases, urotropine and pyridine, to identify the binding configurations of the sample. The adventitious surface carbon, CO type, N-N type, and N-O type from the air were also considered in their analysis. Several groups²⁰⁻²² adopted this method to explain their results on the CN films prepared by different techniques; while some variations in positions and intensities of the respective lines were found. Fujimoto and Ogata²³ found only one single line located at 398.4 eV in the N $1s$ spectra. Other groups^{24,25} proposed that N $1s$ core-level spectra at 400 and 398 eV were attributed to N=C and N \equiv C, respectively. But a comparison to infrared spectra, where N \equiv C bonds were observable at ~ 2200 cm^{-1} ,

showed that there was a minor amount of $\text{N}\equiv\text{C}$ bonds in the CN films.^{26–28} Ronning and his co-workers³ assigned the line at ~ 398 eV to electrons originating from nitrogen atoms having two neighbors, while the line at ~ 400 eV resulting from the electrons in the nitrogen atoms with three neighbors. Normand *et al.*¹ proposed that the method used by Marton¹⁹ was oversimplified to study the real complicated binding configurations of the amorphous CN films, and proposed another way of using the difference between N $1s$ core-level energy and C $1s$ core-level energy to study several kinds of chemical bonds for each lines. In spite of the method of Normand *et al.*, the binding configuration of N and C in the N-doped CNTs will be further resolved in this study.

II. EXPERIMENT

CNTs were synthesized by the assistance of electroplated Pd catalyst²⁹ on the tungsten substrate in an microwave plasma enhanced chemical vapor deposition apparatus with a mixture of methane and hydrogen as precursors.³⁰ The flow rates were maintained at 1 and 100 sccm for methane and hydrogen, respectively. The maximum input power that can be generated in the system is 5 and 2.1 kW was used in this research, and the substrate temperature was at . In order to dope nitrogen atoms, CNTs were further exposed under nitrogen plasma of 3.1 kW microwave input with the nitrogen flow rate at 50 sccm. The high resolution images were studied by transmission electron microscopy (TEM) (Philips TECNA1 20, 200 kV with the LaB_6 filament) and the equipped EELS (Gatan GIF 200TM with the resolution of 0.5 eV) provided the information of carbon binding configurations for CNTs and N-doped CNTs, respectively. The specimens for TEM analysis were prepared by extracting the deposit in ethanol. After ultrasonic treatment for 10 min, a drop of the solution was then dispersed on a carbon-coated Cu grid. The XPS (Perkin-Elmer model PHI 1600) measurements were carried out on the isolated spectrum using the Mg $k\alpha$ x-ray source operating at 250 W. The x-ray source was kept at an incident angle of 54.7° with respect to the analyzer. Energy calibration was done by using the Au $4f_{7/2}$ peak at 83.8 eV. Based on the high-resolution hemispherical analyzer, the energy resolution was 1.6 eV for survey scan spectrum and 0.2 eV for the core-level spectrum, respectively. In order to avoid ion bombardment damage, which would alter the original binding structures and atomic environment in the sample, no ion sputtering was used to do the surface cleaning treatment prior to the XPS measurement. For analysis, appropriate smoothing for the raw data and background removal using the Shirley method³¹ was applied. C $1s$ core-level and N $1s$ core-level spectra were both curve-fitted by the subpeaks with Gaussian and Lorentzian mixed function for the asymmetric core level peak shape.

III. RESULTS AND DISCUSSION

Figures 1(a), 1(c), and 1(d) illustrate the overall structures of CNTs, N doped CNTs doping for 15 and 30 min, respec-

tively. The high-resolution images of (a) and (d) are also shown in Figs. 1(b) and 1(e). The evolution of the structures can be found that the bamboo-like structures are constructed under 15 min nitrogen doping. Bamboo-like structures are mainly composed of the hexagons, pentagons, heptagons, turbostratic graphenes, and a portion of amorphous carbon. These unique structures have been studied for quite some time and familiar to the most scientists today.³² When more and more nitrogen atoms incorporate into the CNTs (doping for 30 min), all the graphene layers are affected and appear seriously distorted resulting in a structure similar to human fingerprints. Waved graphenes, turbostratic structures and fullerene-like structures are all contained inside the N-doped CNTs. In the total energy calculations using semi-empirical Hartree-Fock-based AM1 method,^{33,34} the incorporation of nitrogen atoms into the graphite-like structures would introduce pentagon defects, which distort and bend the graphene layers, leading to graphenes with high curvatures and interlinked structures. According to the calculation proposed by Santos and Alvarez,³⁵ the planarity of the graphite sheet cluster is expected to be buckled when the nitrogen concentration (N/C ratio) exceeds 20%. In our XPS measurements, the N/C ratio of the sample for 15 min nitrogen doping is 10%, while the N/C ratio for 30 min nitrogen doping is 22%. In our results, the nitrogen doping effects on changing the nanostructures of CNTs converge to the conclusion of the references.^{33–35}

C $1s$ core-level and N $1s$ core-level spectra are all shown in Fig. 2 along with the individual fitted subpeaks, respectively. In each figures, the originally raw data, fitted subpeaks and the sum of the fitted subpeaks are all illustrated. During the spectra analysis, we accept the fitted results with the lowest value of chi-square (χ^2),³¹ on the premise that the fit makes chemical and spectroscopic sense in the meantime. Four lines were assigned to fit the C $1s$ core, and two lines for N $1s$ core. Increasing or decreasing the amount of subpeaks for each core level spectrum cannot improve the analysis results furthermore. In the C $1s$ core spectra, line C_1 is identified as adventitious carbon and surface carbon, and line C_4 is identified as CO type bonds, both of which are similar to the Marton's¹⁹ although some variation in positions and intensities of the respective lines are noted in our case. In order to identify the nitrogen binding configurations for N_1 and N_2 , we calculate the energy difference between N $1s$ core and C $1s$ core level energies, e.g., values of (N_1-C_2) and (N_2-C_2) , according to the work of Normand *et al.*¹ By referring to the core level energy differences for several chemical bond types,^{1,36,37} we can distinguish what kind of the binding configurations of N_1 and N_2 lines belong to. Figure 3 shows the identification results for the 30 min nitrogen doped CNTs, in which dashed lines are the original analysis while the solid lines are associated with appropriate modifications. At the first stage, we found that the value of (N_1-C_2) equals to 112.3 eV, which lies below the energy difference of nitrile bonds (112.84 eV), while the value of (N_2-C_2) equals to 113.3 eV, which lies near the energy difference of poly 4-vinylpyridine (P4VP) type (113.35 eV). According to this, the N_1 line is suspected to be the $\text{N}\equiv\text{C}$ bond and the N_2 line could be the pyridine-like

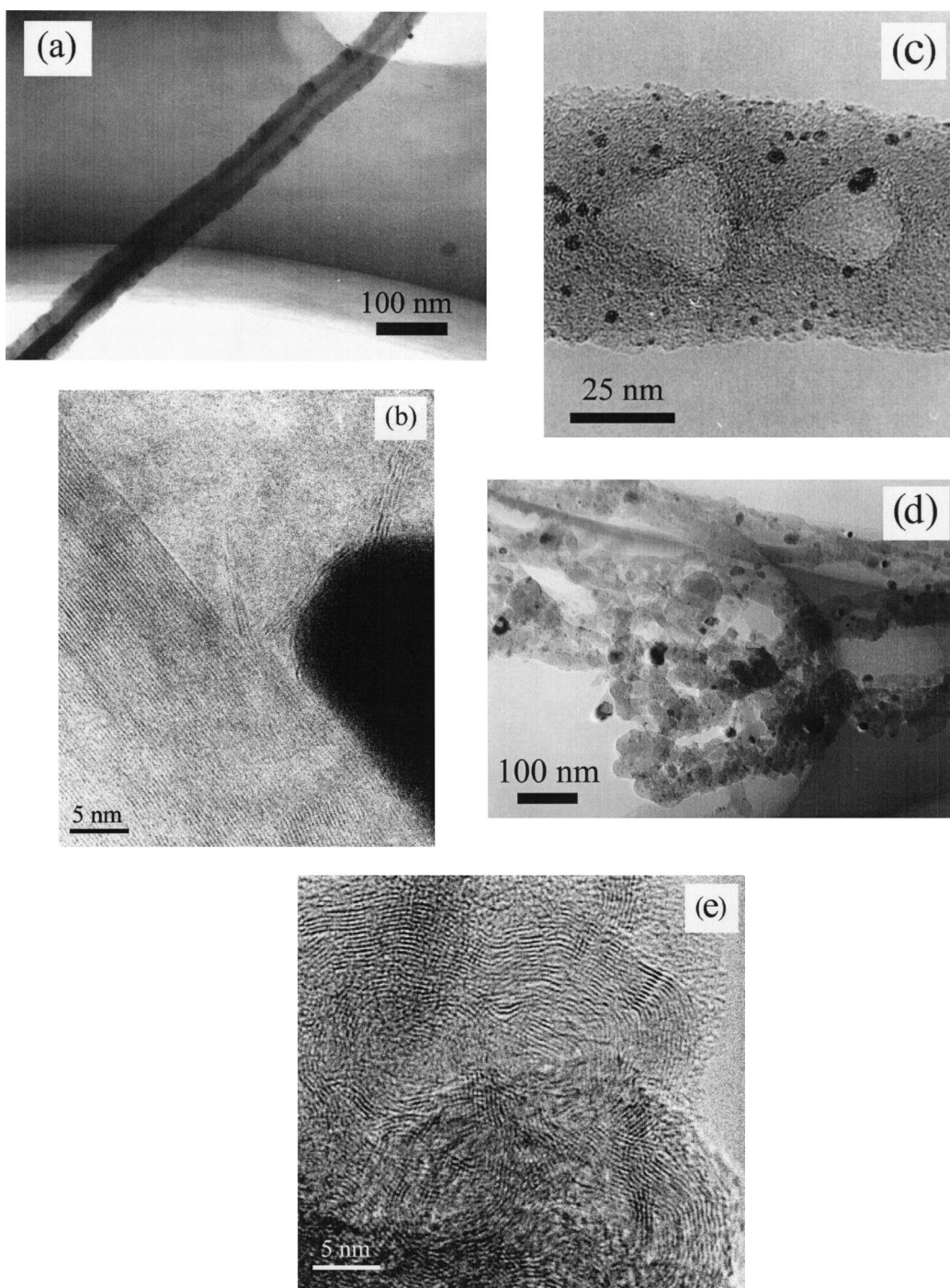


FIG. 1. The overall structures of (a) CNTs (no doping), (c) N-doped CNTs (doping for 15 min), and (d) N-doped CNTs (doping for 30 min), while the respective high-resolution images of (a) and (d) are illustrated in (b) and (e).

binding type. Unfortunately, it is skeptical that whether the method of Normand *et al.*¹ could absolutely meet our requirements and exactly have the correct interpretation in our N-doped CNTs case, compared with the FTIR measurements as shown in Fig. 4(c), in which two bands appear at ~ 1235 and 1590 cm^{-1} , but no band at $\sim 2200\text{ cm}^{-1}$ detected. The band at $\sim 1200\text{ cm}^{-1}$ is attributed to N-C or C-O stretching modes, at $\sim 1500\text{ cm}^{-1}$ belongs to N=C stretching mode and at $\sim 2200\text{ cm}^{-1}$ corresponds to N \equiv C stretching mode. Results of FTIR exclude the existence of

N \equiv C binding configurations of nitrogen in the N-doped CNTs and, however, some modifications should be taken into consideration. The analyzed results of 15 min nitrogen doped CNTs are also similar. The value of (N_1 -C₂) and (N_2 -C₂) is equal to 112.7 and 113.4 eV, respectively. FTIR spectrum in Fig. 4(b) also excludes the existence of N \equiv C binding configurations.

The maximum nitrogen peak positions for the nitrogen-doped carbon related materials and carbon nitride films in most published results lay in the range of

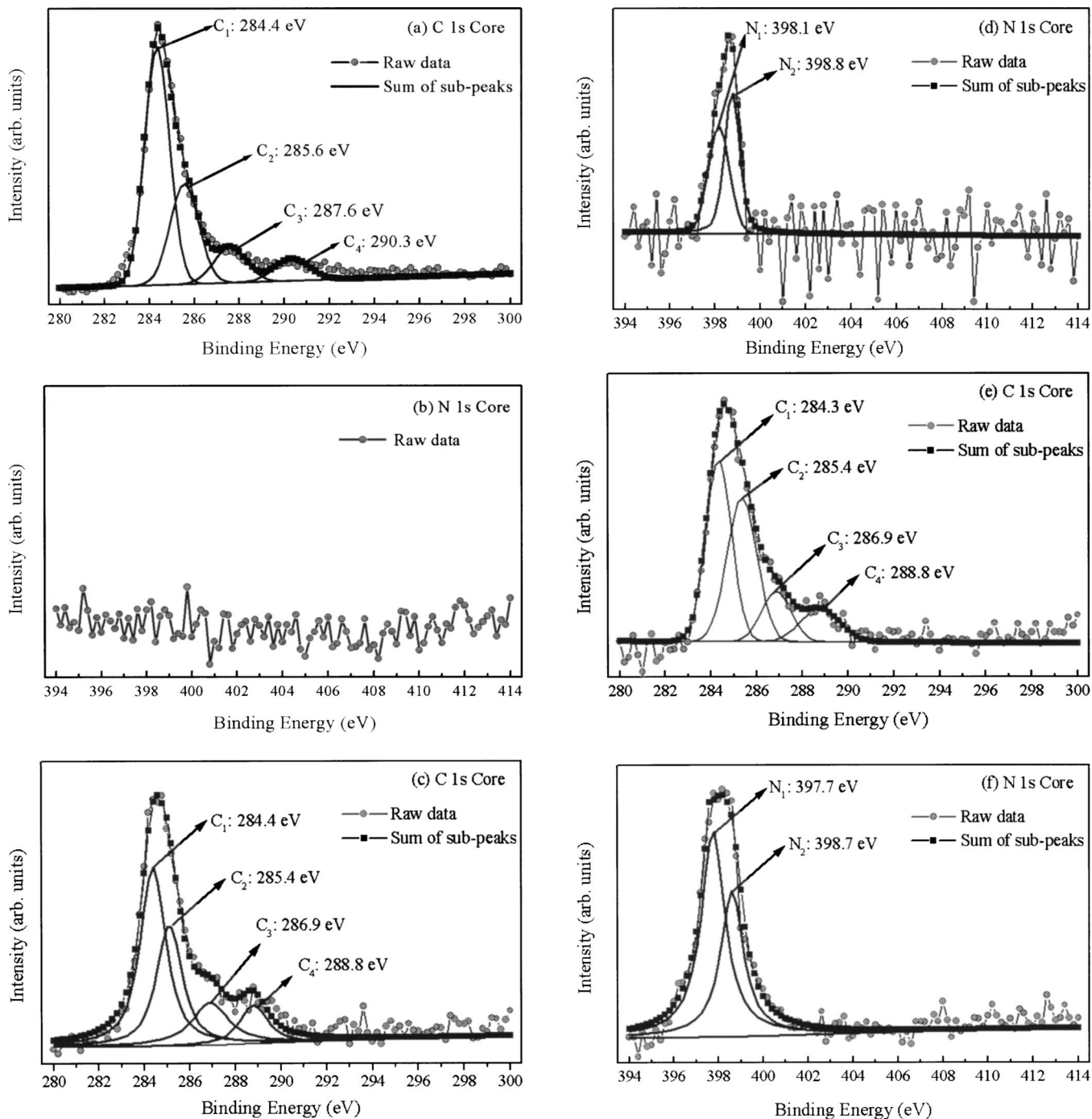


FIG. 2. XPS measurements of C 1s and N 1s core-level spectra for various CNTs: (a) and (b) for CNTs without doping; (c) and (d) for 15 min N-doped CNTs; (e) and (f) for 30 min N-doped CNTs. Four subpeaks were applied to curve-fit C 1s core and two subpeaks to curve-fit N 1s core, and the values of (N_1-C_2) and (N_2-C_2) are applied to identify the binding configurations of nitrogen.

398–401 eV,^{1,9,18,38,39} while our results are all 1 eV downshift, as shown in both Figs. 2(d) and 2(f). Such an 1 eV downshift could be attributed to several reasons summarized as follows.

(1) Chemical shift: The chemical shift is due to the different chemical environments for nitrogen atoms in various compounds.

(2) Relaxation effect: The binding energy of the core level K photoelectron escaping the solid surface can be ex-

pressed by the general framework of the charge potential model^{1,40,41}

$$E_b^{\text{vac}}(K) = E_{b,0}^{\text{vac}}(K) + k(K)q_i + \sum_{j \neq i} (q_j/r_{ij}) - E_{\text{relax}}(K),$$

where $E_{b,0}^{\text{vac}}(K)$ is the binding energy referenced to the vacuum level of a reference state; $k(K)q_i$ is a term of polarization of the bond; $\sum_{j \neq i} (q_j/r_{ij})$ is the electrostatic potential of Madelung's type; and $E_{\text{relax}}(K)$ is contributed

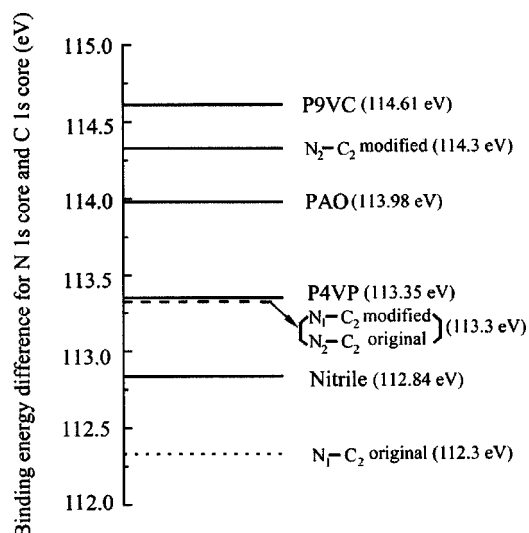


FIG. 3. Schematic representation for the identification of (N_1-C_2) and (N_2-C_2) in N doped CNTs (doping for 30 min) with respect to the core level energy difference of various binding types (dashed lines are the original analysis without any modification and solid lines with appropriate modifications of 1 eV adding to compensate the relaxation effects).

from the relaxation effects due to the core hole in the final state.

When one nitrogen atom sp^2 hybridizes the carbon atom in N-doped CNTs, in principle, the delocalized electrons in the π bond would screen the electron holes produced in carbon and nitrogen atoms. Because of the larger electronegativity of nitrogen than that of carbon, the electron cloud of the CN covalent bonds has the tendency to move toward the nitrogen atom. At first, this charge transfer behavior itself will decrease the nitrogen binding energy and raise the carbon binding energy. Second, the electron cloud moving toward the nitrogen atom makes the screening effect more obvious in the nitrogen atom than in the carbon atom. By combining the charge transfer and the screening effect, the binding energy of the carbon atom could either be increased or decreased depending on the compensation results of these two effects, while the binding energy of the nitrogen atom can be largely decreased due to these two effects. Thus, additional mechanisms which can enhance the screening effect are also helpful to reduce the nitrogen binding energy.

(3) Increasing sp^2 binding: Delocalized electrons in the π bond of sp^2 hybridization can move easier than the highly localized electrons in the σ bond; thus electrons in sp^2 hybridization can more actively participate in the screening of the core holes. In EELS measurements as shown in Fig. 5, the pre-edge of the carbon peak corresponding to the $1s$ to π^* transition is apparently enhanced with the increased nitrogen amount doped in CNTs. Because the $N\equiv C$ stretching mode is excluded in our case (for the absence of the band at ~ 2200 cm^{-1} in FTIR results), the signal resulting from the $1s$ to π^* transition comes mainly from the sp^2 binding. Figure 5 also indicates that the nitrogen incorporation into CNTs would increase the degree of sp^2 binding, which also fits with the published works.^{2,3} Since sp^2 binding

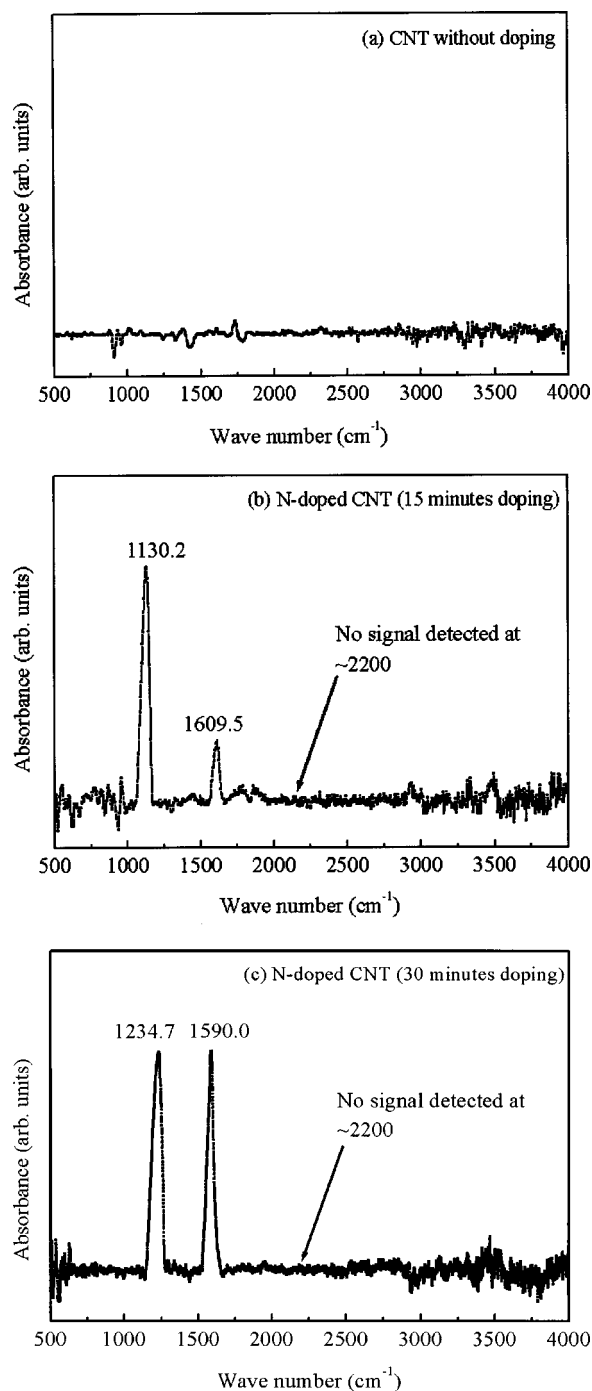


FIG. 4. FTIR spectrum for (a) CNTs (no doping), (b) N-doped CNTs (doping for 15 min), and (c) N-doped CNTs (doping for 30 min); no signal detected at ~ 2200 cm^{-1} implying that $N\equiv C$ stretching mode can be neglected in our case.

in N-doped CNTs is increased, the relaxation effect due to the screening of the core holes by electrons is therefore reinforced.

(4) Highly distorted graphenes: CNTs are rolled up mainly by graphene layers that are composed of purely sp^2 binding carbon atoms. When the graphene layers are seriously distorted and waved such as seen in Fig. 1(e), the tendency or probability of tangling and folding for the graphene layers in the three-dimensional spaces would increase. This

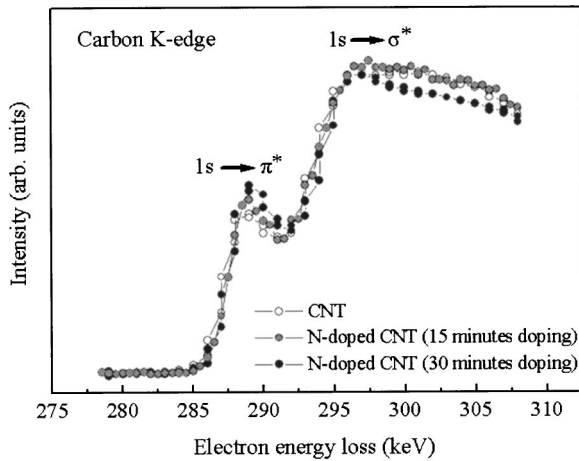


FIG. 5. EELS results of carbon *K* edge for CNT and for N-doped CNTs (doping for 15 and 30 min), indicating that the intensity of $1s$ to π^* transition is raised with the increased amount of nitrogen doping in CNTs, implying that the nitrogen incorporating into the CNTs would increase the amount of sp^2 binding type.

implies that the wrapping of graphene layers will increase the probability of folded sp^2 bindings in the space, thereby enhancing the mobility of electrons in the π bonds, which in turn increases the relaxation effects.

In order to identify the binding structures in our system, an adjustment by adding 1 eV to both (N_1-C_2) and (N_2-C_2) values is done to compensate for the downshift effect in order to trace the nitrogen binding types. The newly adjusted value of (N_1-C_2) at 113.3 eV lies near the P4VP type, while the newly adjusted value of (N_2-C_2) at 114.3 eV locates between the poly aniline oligomer (PAO) and poly 9-vinylcarbazole (P9VC) types, as indicated by the solid lines in Fig. 3. From the earlier analysis, the N_1 line is associated with the nitrogen atoms having two neighbors (like P4VP) and the N_2 line comes from the nitrogen atom having three neighbors (like PAO and P9VC). In other words, the N_1 line (the lower binding energy in the N $1s$ core) is assigned

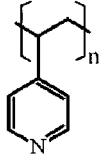
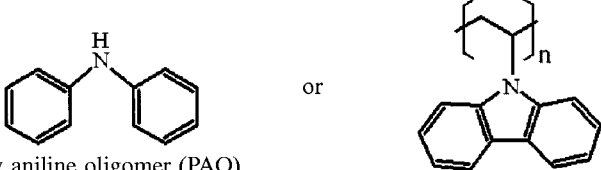
to be the nitrogen atom sp^2 hybridizing the other atoms, while the N_2 line (the higher binding energy in the N $1s$ core) is the nitrogen atoms sp^3 hybridizing the other atoms. The results of XPS analysis are similar to the published works.^{3,42} Distinct from other nitrogen contained carbon-based materials, interpretation of the binding structures for both the N_1 and N_2 line in N-doped CNTs should start from considering the original characteristic nanostructures of the CNTs, which are constructed by rolling up the plural hexagonal graphene layers to form the concentric cylinders. When nitrogen atoms incorporate into the CNTs, it is easy for them to substitute carbon atoms in the hexagon network without raising too much strain energy because of the smaller difference in atomic radii for these two atoms. The N_1 line means that one nitrogen substitute one carbon atom in the hexagon graphene without changing the hexagon shape but allowing the neighboring hexagon to have dangling bonds due to the four hybrid orbitals for carbon while three hybrid orbitals for nitrogen. The N_2 line contains two types of the binding configurations: PAO and P9VC types. It is interpreted that in the PAO type, a nitrogen atom can intercalate between the two graphene layers and crosslink the graphene layers, while in the P9VC type, a nitrogen can introduce the pentagon defect inside the hexagon network. Theoretical predictions and experiments³³⁻³⁵ also support our analysis results. The earlier discussion is summarized in Table I.

In the C $1s$ core level spectrum, it is suggested that C_2 and C_3 should be contributed from the sp^2 and sp^3 hybridized carbons, respectively, in comparison with the EELS results and other published results of the carbon films.⁴³ The integrated area ratio of C_2/C_3 increases from 2.49 to 2.86 for CNTs and for N-doped CNTs (doping for 30 min), respectively. The result of EELS shows the same tendency, i.e., the intensity of $1s$ to π^* transition is raised in N-doped CNTs.

IV. CONCLUSIONS

In conclusion, we are able to analyze the N $1s$ core level spectrum for N-doped CNTs by using the modified approach

TABLE I. Summarized table for the binding configuration of nitrogen atoms in the N-doped CNTs.

| Peaks | Binding types | N atoms in the N-doped CNTs |
|-------|--|--|
| N_1 |  poly 4-vinylpyridine (P4VP) | One nitrogen atom substitutes one carbon atom in the hexagon graphene |
| N_2 |  poly aniline oligomer (PAO) or poly 9-vinylcarbazole (P9VC) | (1) Nitrogen can intercalate between two graphene layers and crosslink the graphene layers (2) Nitrogen can introduce the pentagon inside the network |

of Normand *et al.*¹ in combination with the FTIR and EELS measurements. The N_1 line results from nitrogen atom substituting the carbon atom located in the hexagon graphene, while the N_2 line is identified as two binding configurations of the nitrogen atoms, which crosslink the graphene layers and introduce the pentagon defect into the hexagon network of carbon, respectively.

ACKNOWLEDGMENTS

The authors would like to acknowledge the support of this work by the National Science Council of the Republic of China under Contract No. NSC91-2120-E-007-006. The authors would also like to acknowledge Professor F. S. Shieu for assistance of valuable discussion.

- *Author to whom correspondence should be addressed; Fax: 886-3-5710290. Email address: hcshih@mse.nthu.edu.tw
- ¹F. L. Normand, J. Hommet, T. Szörényi, C. Fuchs, and E. Fogarassy, *Phys. Rev. B* **64**, 235416 (2001).
 - ²J. Hu, P. Yang, and C. M. Lieber, *Phys. Rev. B* **57**, R3185 (1998).
 - ³C. Ronning, H. Feldermann, R. Merk, and H. Hofsäuss, *Phys. Rev. B* **58**, 2207 (1998).
 - ⁴S. Iijima, *Nature (London)* **354**, 56 (1991).
 - ⁵K. Tanaka, T. Yamabe, and K. Fukui, *The Science and Technology of Carbon Nanotubes*, 1st ed. (Elsevier Science, New York, 1999).
 - ⁶D. L. Carroll, Ph. Redlich, X. Blasé, J.-C. Charlier, S. Curran, P. M. Ajayan, S. Roth, and M. Ruhle, *Phys. Rev. Lett.* **81**, 2332 (1998).
 - ⁷M. Torriones, W. K. Hsn, A. Schilder, H. Terrones, N. Crobert, J. P. Hare, Y. Q. Zhu, M. Schwoerer, K. Prassides, H. W. Kroto, and D. R. M. Walton, *Appl. Phys. A: Mater. Sci. Process.* **A66**, 307 (1998).
 - ⁸O. Stephan, P. M. Ajayan, C. Colliex, P. Redlich, J. M. Lambert, P. Bernier, and P. Lefin, *Science* **266**, 1683 (1994).
 - ⁹M. Terrones, P. Redlich, N. Grobert, S. Trasobares, W.-K. Hsu, H. Terrones, Y.-Q. Zhu, J. P. Hare, C. L. Reeves, A. K. Cheetham, M. Rühle, H. W. Kroto, and D. R. M. Walton, *Adv. Mater. (Weinheim, Ger.)* **8**, 655 (1999).
 - ¹⁰T. Laude, Y. Matsui, A. Marraud, and B. Jouffrey, *Appl. Phys. Lett.* **76**, 3239 (2000).
 - ¹¹L. H. Chan, K. H. Hong, D. Q. Xiao, T. C. Lin, W. J. Hsieh, S. H. Lai, F. S. Shieu, and H. C. Shih, *Appl. Phys. Lett.* **82**, 4334 (2003).
 - ¹²W. Han, Y. Bando, K. Kurashima, and T. Sato, *Appl. Phys. Lett.* **73**, 3085 (1998).
 - ¹³D. Golberg, Y. Bando, W. Han, K. Kurashima, and T. Sato, *Chem. Phys. Lett.* **308**, 337 (1999).
 - ¹⁴A. Y. Liu and M. L. Cohen, *Science* **245**, 841 (1989).
 - ¹⁵A. Y. Liu and M. L. Cohen, *Phys. Rev. B* **41**, 10 727 (1990).
 - ¹⁶S. L. Sung, S. H. Tsai, C. H. Tseng, F. K. Chiang, X. W. Liu, and H. C. Shih, *Appl. Phys. Lett.* **74**, 197 (1999).
 - ¹⁷X. W. Liu, C. H. Tseng, J. H. Lin, L. T. Chao, and H. C. Shih, *Surf. Coat. Technol.* **135**, 184 (2001).
 - ¹⁸S. L. Sung, T. G. Tsai, K. P. Huang, J. H. Huang, and H. C. Shih, *Jpn. J. Appl. Phys., Part 1* **37**, 148 (1998).
 - ¹⁹D. Marton, K. J. Boyd, A. H. Al-Bayati, S. S. Todorov, and J. W. Rabalais, *Phys. Rev. Lett.* **73**, 118 (1994).
 - ²⁰A. K. Sharma, P. Ayyub, M. S. Multani, K. P. Adhi, S. B. Ogale, M. Sunderaraman, D. D. Upadhyay, and S. Banerjee, *Appl. Phys. Lett.* **69**, 3489 (1996).
 - ²¹M. Tabbal, P. Merel, S. Moisan, M. Chaker, A. Ricard, and M. Moisan, *Appl. Phys. Lett.* **69**, 1698 (1996).
 - ²²A. Bousetta, M. Lu, and A. Bensaoula, *J. Vac. Sci. Technol. A* **13**, 1639 (1995).
 - ²³F. Fujimoto and K. Ogata, *Jpn. J. Appl. Phys., Part 2* **32**, L420 (1993).
 - ²⁴L. Galan, I. Montero, and F. Rueda, *Surf. Coat. Technol.* **83**, 103 (1996).
 - ²⁵P. V. Kela, D. C. Cameron, B. J. Meenan, K. A. Pischow, C. A. Anderson, N. M. D. Brown, and M. S. J. Hashmi, *Surf. Coat. Technol.* **74-75**, 696 (1995).
 - ²⁶S. Kobayashi, S. Nozaki, H. Morisaki, S. Fukui, and S. Masaki, *Thin Solid Films* **281-282**, 289 (1996).
 - ²⁷P. Hammer, M. A. Baker, C. Lenardi, and W. Gissler, *J. Vac. Sci. Technol. A* **15**, 107 (1997).
 - ²⁸H. Xin, C. Lin, S. Zhu, S. Zou, X. Shi, H. Zhu, and P. L. F. Hemment, *Nucl. Instrum. Methods Phys. Res. B* **103**, 309 (1995).
 - ²⁹S. H. Tsai, C. L. Lee, C. W. Chao, and H. C. Shih, *Carbon* **38**, 781 (2000).
 - ³⁰S. H. Tsai, C. W. Chao, C. L. Lee, and H. C. Shih, *Appl. Phys. Lett.* **74**, 3462 (1999).
 - ³¹D. Briggs and M. P. Seah, *Practical Surface Analysis Volume 1: Auger and X-ray Photoelectron Spectroscopy*, 2nd ed. (Wiley, New York, 1990).
 - ³²T. W. Ebbesen, *Carbon Nanotubes: Preparation and Properties*, 1st ed. (CRC Press, New York, 1997).
 - ³³M. J. S. Dewar, E. G. Zoebisch, E. F. Mealy, and J. J. P. Stewart, *J. Am. Chem. Soc.* **107**, 3902 (1985).
 - ³⁴H. Sjöström, S. Stafström, M. Boman, and J.-E. Sunogren, *Phys. Rev. Lett.* **75**, 1336 (1995).
 - ³⁵M. C. D. Santos and F. Alvarez, *Phys. Rev. B* **58**, 13 918 (1998).
 - ³⁶G. Beamson and D. Briggs, *High Resolution XPS on Organic Compounds* (Wiley, Chichester, UK, 1992).
 - ³⁷J. Schafer, J. Ristein, R. Graupner, L. Ley, U. Stephan, T. Frauenheim, V. S. Veerasamy, G. A. J. Amaratunga, M. Weiler, and H. Ehrhardt, *Phys. Rev. B* **53**, 7762 (1996).
 - ³⁸C. Quirós, J. G. Garcia, F. J. Palomares, L. Soriano, E. Elizalde, and J. M. Sanz, *Appl. Phys. Lett.* **77**, 803 (2000).
 - ³⁹X. W. Liu, S. H. Tsai, L. H. Lee, M. X. Yang, A. C. M. Yang, I. N. Lin, and H. C. Shih, *J. Vac. Sci. Technol. B* **14**, 1840 (2000).
 - ⁴⁰M. Cardona and L. Ley, *Photoemission in Solids I* (Springer-Verlag, Berlin, 1978).
 - ⁴¹W. F. Egelhoff Jr., *Surf. Sci. Rep.* **6**, 323 (1986).
 - ⁴²A. Snis and S. F. Matar, *Phys. Rev. B* **60**, 10 855 (1999).
 - ⁴³R. Haerle, E. Riedo, A. Pasquarello, and A. Baldereschi, *Phys. Rev. B* **65**, 045101 (2001).